Spin crossover in mixed-anion Fe(NH 2 trz) 3 (BF 4)(SiF 6) 0.5 crystalline rod-shaped particles: the strength of the solid–liquid post synthetic modification

Xinyu Yang, Alejandro Enriquez-Cabrera, Dorian Toha, Yannick Coppel, Lionel Salmon, Azzedine Bousseksou

Spin crossover in mixed-anion $Fe(NH_2trz)_3(BF_4)(SiF_6)_{0.5}$ crystalline rod-shaped particles: the strength of the solid-liquid post synthetic modification

Xinyu Yang, Alejandro Enriquez Cabrera, Dorian Toha, Yannick Coppel, Lionel Salmon, Azzedine Bousseksou**

[1]*LCC, CNRS & Université de Toulouse (UPS, INP), 31077 Toulouse, France*

***** lionel.salmon@lcc-toulouse.fr, azzedine.bousseksou@lcc-toulouse.fr

Keywords: spin crossover, iron(II), Triazole, TEOS, PSM, MAS NMR

Abstract

A pure mixed-anion $Fe(NH_2trz)_3(BF_4)(SiF_6)_{0.5}$ spin crossover complex is obtained implementing a solid-liquid post synthetic modification approach from the $Fe(NH_2trz)_3(BF_4)_2$ parent complex. This method allows obtaining highly crystalline powder samples incorporating homogeneous micrometric (1 µm long) rod-shaped particles. This compound presents an abrupt spin crossover behaviour with a narrow (10 K) hysteresis loop centred just above room temperature (320 K) which makes it very interesting for future integration into devices for various applications.

1. Introduction

Molecular spin crossover (SCO) complexes are phase change materials that exhibit variable multi-properties upon stimulus like a temperature variation and have been proposed as active elements in various, optical, electrical and mechanical devices [1-5]. Since the discovery of the phenomenon in 1931 [6], numerous examples of SCO complexes with various physical properties have been reported in the literature for different 3d metals [7-12]. Indeed, the ligand field around certain d metal complexes, the crystal packing and specific supramolecular interactions between SCO molecules can give rise to a diversity of spin conversion behavior ranging from gradual to cooperative with or without bistability domain and at different temperatures spanning from 80 to 500 K [13-15]. Nevertheless, there is still an expectation to obtain stable and integrable compounds with transition temperatures just above room temperature, with or without hysteresis loop to confer or not a memory effect in order to target functional applications. One of the most studied class of iron(II) compounds belongs to the Fe-triazole family with iron ions forming 1D chains incorporating three neutral triazole bridging ligands; where the positive charge of the metal centers is counterbalanced by the presence of counter anions interspersed between the chains [16,17]. One of the strategies developed to modify the spin transition temperature consisted of partially substituting either the ligand or the metal within these coordination complexes [18-21]. In particular, the dilution of iron with SCO inactive metal (zinc) complex led to the decrease of the transition temperatures as well as the reduction of the cooperativity between iron centers affording reduced-width hysteresis and/or conversion with more gradual characters. This ‘molecular alloying’ approach has been explored both with bulk and nano-sized SCO materials [22-25]. In general, the approach developed to substitute the selected element (metal center or ligand) consisted simply to mix the corresponding precursors, with specific amounts to modulate the final chemical composition of the product. In fact, no result was reported on the synthesis of the corresponding pure mixed

counter-anion derivatives. Note that only a powder mixture of $Fe(NH_2trz)_3(BF_4)(SiF_6)_{0.5}$ and $Fe(NH_2trz)_3(BF_4)_2$ complexes was reported showing the occurrence of a two-step spin transition reflecting the independent properties for each complex [26]. In this case, the hardly controllable anion substitution can be explained by the ability of the BF_4^- anion to dissociate into hydrofluoric acid, the latter reacting with the glass tube (SiO_2) to form the SiF_6^{2-} anions, which are then in competition with the BF_4^- anions in the solution during the formation of the $Fe(NH_2trz)_3(BF_4)_2$ complex. Moreover, X-ray diffraction study revealed the crystal structure of $Fe(NH_2trz)_3(BF_4)(SiF_6)_{0.5}$ [26]. Our group and others have used tetraethyl orthosilicate (TEOS) as a SiO_2 precursor in reverse micelle syntheses to elaborate functionalized core@shell $[Fe(Htrz)_2\text{-}trz](BF_4)@SiO_2$ nanoparticles [23, 27-31]. In the latter cases, the exchange of the BF_4^- by the SiF_6^{2-} was not observed revealing certainly the key role play by the NH_2trz ligand in the substitution mechanism. Shepherd and collaborators recently used a solid-solid post synthetic modification (PSM) grinding method to fully substitute halogen counter-anions in similar iron(II) 1,2,4-triazole based spin crossover materials [32]. On the other hand, solid-liquid [33] and solid-vapor [34-37] post synthetic modifications have been also reported for this family of complexes. In particular, we have demonstrated that playing with the experimental conditions, both partial but more importantly complete solid-liquid PSM can be obtained from the $[Fe(NH_2trz)_3](NO_3)_2$ derivative by reaction of the ligand with different substrates [38]. The aim of the hereafter reported work is to synthesize a pure mixed counter-anion compound and to determine the effect of the anion mixing on the spin transition temperatures of the complex while comparing the implementation of both conventional synthetic and solid-liquid PSM methods.

2. Experimental section

2.1 Sample characterization

Elemental analyses of C, H, and N were performed by means of a Perkin–Elmer 2400 series II device after combustion at 850 °C, using IR detection and gravimetry. Elemental analyses of Fe and B were carried out using a Thermo Scientific ICAP 6300 inductively coupled plasma atomic emission spectrometer (ICP-AES). NMR experiments were recorded on a Bruker Avance 400 III HD spectrometer operating at magnetic fields of 9.4 T. Samples were packed into 3.2 mm rotor and spun at different spinning rate (typically between 8 to 16 kHz) at low temperature (between 263 K to 193 K). ^{19}F were measured with Hahn-echo scheme synchronized with the spinning rate and relaxation delay of 2 s. ^{11}B MAS have been acquired with single pulse experiments with recycle delays of 2 s. Chemical shifts were externally referenced to $BF_3.Et_2O$ and CCl_3F for ^{11}B and ^{19}F, respectively. Thermogravimetric analyses (TGA) were conducted in an inert nitrogen atmosphere using a Mettler Toledo 3+ thermal analyser. The size and morphology of the SCO particles were determined by transmission electron microscopy (TEM) using a JEOL JEM-1011. TEM samples were prepared by placing a drop of the particles (suspended in ethanol) on a carbon-coated copper grid. Powder X-ray diffraction patterns were recorded using a PANalytical X'Pert equipped with a Cu X-ray tube, a Ge(111) incident beam monochromator (λ = 1.5406 Å) and an X'Celerator detector. Variable-temperature optical reflectivity data were acquired with a MOTIC SMZ-168 stereomicroscope equipped with MOTICAM 1000 color CMOS camera. A 2 K min^{-1} rate was used for both cooling and heating. Magnetic susceptibility data were collected with a Quantum Design MPMS-XL SQUID magnetometer at heating and cooling rates of 2 K min^{-1} in a magnetic field of 1 kOe. The magnetic data were corrected for the diamagnetic contribution.

2.2. Synthesis of the spin crossover complex

All reagents were purchased from Sigma Aldrich and used without further purification. All the reactions were performed in plastic containers (centrifugal Falcon tubes). $[Fe(NH_2trz)_3](BF_4)_2 \cdot yH_2O$ was synthesized by dissolving 0.746 g of 4-NH_2-1,2,4-triazole in 3.5 mL of water. In a separated flask, 1 g of $Fe(BF_4)_2 \cdot 6H_2O$ was dissolved in 3.5 mL of water. The iron solution was added slowly to the triazole ligand solution and the mixture was stirred for 24 hours at room temperature resulting in a white precipitate. The product was purified by three successive ethanol washing/centrifugation cycles resulting in 1.14 g of a white solid (80 % yield). Thermogravimetry analysis revealed the inclusion of 0.6 molecules of water and the thermal stability of the complex up to ca. 240 °C (see **Fig. S1** in the Supporting Information, SI) Elemental analyses calculated for $[Fe(NH_2trz)_3](BF_4)_2 \cdot 0.6H_2O$ (**1**, Mw = 492.5 g/mol): C, 14.6; H, 2.7; N, 34.1; Fe 11.3; B 4.4 %. Found: C, 14.7; H, 2.0; N, 33.9; Fe 11.0; B 4.2 %. The thermal variation of the reflectance, shown in **Fig. S4,** revealed abrupt spin transitions at 240 K and 230 K for heating and cooling, respectively, in agreement with previous reports [39].

$[Fe(NH_2trz)_3](BF_4)_{2-x}(SiF_6)_{x/2} \cdot yH_2O$ was synthesized by dissolving 0.2 g of $Fe(BF_4)_2 \cdot 6H_2O$ in 2 mL in a plastic flask and adding successively 0.036 g (0.3 eq) of TEOS and 0.149 g (3 eq) of 4-NH_2-1,2,4-triazole resulting in an immediate precipitate. The suspension was stirred overnight and the product purified by three successive ethanol washing/centrifugation cycles resulting in 0.178 g of a pink solid (61 % yield). Thermogravimetry analysis revealed the inclusion of 0.85 molecules of water and the thermal stability of the complex up to ca. 230°C (see **Fig. S1** in the Supporting Information, SI) Elemental analyses calculated for $[Fe(NH_2trz)_3](BF_4)_{1.2}(SiF_6)_{0.4} \cdot 0.85H_2O$ (**2**, Mw = 484.4 g/mol): C, 14.9; H, 2.8; N, 34.7; Fe, 11.5; B, 2.7 %. Found: C, 14.9; H, 1.9; N, 34.4; Fe, 11.8; B, 2.8 %. For the PSM reaction, 0.133 g of **1** was suspended in 1 mL of water at room temperature and 0.017 g of TEOS (0.3 eq) was added. The white suspension was stirred during 1 week, showing a progressive color change

from white to pink and leading after three successive ethanol washing/centrifugation cycles to 0.093 g of a pink solid (72 % yield). Thermogravimetry analysis revealed the inclusion of 0.6 molecules of water and the thermal stability of the complex up to ca. 230°C (see **Fig. S1** in the Supporting Information, SI) Elemental analyses calculated for $[Fe(NH_2trz)_3](BF_4)_1(SiF_6)_{0.5}\cdot 0.6H_2O$ (**3**, Mw = 476.7 g/mol): C, 15.1; H, 2.8; N, 35.2; Fe, 11.7; B, 2.3 %. Found: C, 15.1; H, 1.8; N, 34.2; Fe, 11.9; B, 2.7 %.

3. Results and discussion

In order to produce a pure powder form of the mixed-anion $Fe(NH_2trz)_3(BF_4)_{2-x}(SiF_6)_{x/2}$ complex, TEOS was used as reagent and SiF_6^{2-} precursor in "classic" coordination reaction and solid-liquid PSM; as shown in **scheme 1**. In both cases, the reaction is performed in plastic container to avoid competition with the SiO_2 ripped from the wall of the glass container. The synthesis of the preliminary complex $[Fe(NH_2trz)_3](BF_4)_2$ **1** was already reported and the white color of the obtained solid at room temperature is in agreement with a HS state for the iron(II) center and a spin crossover behavior below room temperature (*vide-infra*) [26].

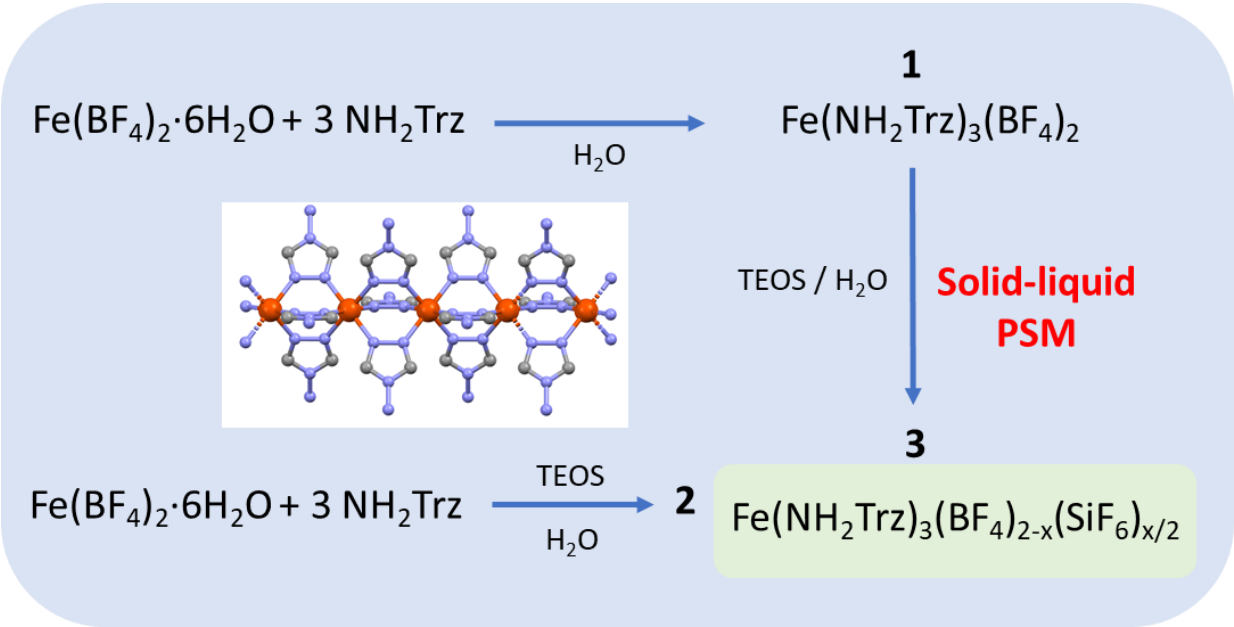

Scheme 1: Reaction scheme and representation of the 1D "Fe-triazole" chains

The preparation of sample **2** and **3** is carried out by bulk synthesis and post synthetic modification, respectively, using 0.3 eq of TEOS (versus iron) and affording similar pink powder samples. Samples **1**-**3** were characterized by infrared spectroscopy which revealed in addition to the well-known vibration modes of torsion and stretching deformation of the triazole ring around 600-650 cm^{-1} and 1500-1550 cm^{-1}, respectively, the characteristic vibration modes of the different counter-anions (See **Fig. S2** of the SI). For sample **1**, an intense band attributed to the BF_4^- anions is observed at 1000 and 1095 cm^{-1}. This latter vibration mode is also present on the IR spectrum of samples **2** and **3** but seems to be split at 1078 and 1102 cm^{-1} that could correlate the presence of two different BF_4^- sites in the structure. As expected, the ν3 absorption band characteristics of the SiF_6^{2-} ion appears at 730 cm^{-1} and is more intense for sample **3** compared to sample **2** revealing a higher cations exchange in sample **3**. The fine composition of all complexes was determined coupling thermogravimetric and elemental analyses leading to the following formulae: $[Fe(NH_2trz)_3](BF_4)_2 \cdot 0.6H_2O$ (**1**), $[Fe(NH_2trz)_3](BF_4)_{1.2}(SiF_6)_{0.4} \cdot 0.85H_2O$ (**2**) and $[Fe(NH_2trz)_3](BF_4)_1(SiF_6)_{0.5} \cdot 0.6H_2O$ (**3**). Consistent with the reduce yields, the high content of SiF_6^{2-} in the products (compared to the 0.3 eq of TEOS used) can be explain by the formation of intermediate species from $BF_3(OH)^-$ to $B(OH)_3$ which stay in solution, making BF_4^- the limiting species.

Solid-state nuclear magnetic resonance (SSNMR) has established its status as one of the most powerful methods to characterize non-crystalline materials [40]. In the solid state, the absence of the fast tumbling motions on the NMR timescale leads to broad NMR resonances associated with anisotropic magnetic interactions (chemical shift anisotropy, dipolar couplings…) in contrast to solution NMR. The resolution of the SSNMR spectra can be greatly improved by using the magic angle spinning technique (MAS). MAS SSNMR with high-resolution have demonstrated clear benefits for obtaining large signal sensitivity gain and probing spin dynamics phenomena [41,42]. However, MAS spinning results to a temperature increase of the

sample because of the friction between the air and the rotating rotor. **Figure 1** reports selected ^{19}F Hahn-echo MAS and ^{11}B MAS spectra for various spinning frequencies (ν_r) and temperatures for sample **2** and **3** (see also **Fig. S4** for complementary data). Concerning ^{19}F NMR spectrum, the increase of ν_r from 6 to 11.3 kHz, is not enough to clearly separate the isotropic signals of the two counter-anions from their sidebands associated to chemical shift anisotropy. Unfortunately, a further increase to 14.3 kHz shows a strong degradation of the signals with broadening and appearance of many additional sidebands. These effects are associated with magnetic interactions between nuclear and electron spins indicating the material adopt a paramagnetic behaviour. It is in agreement with the fact that the complex presents a mixed LS/HS state when the temperature increase to ca. 323 K (see hereafter the thermal variation of the optical reflectance).

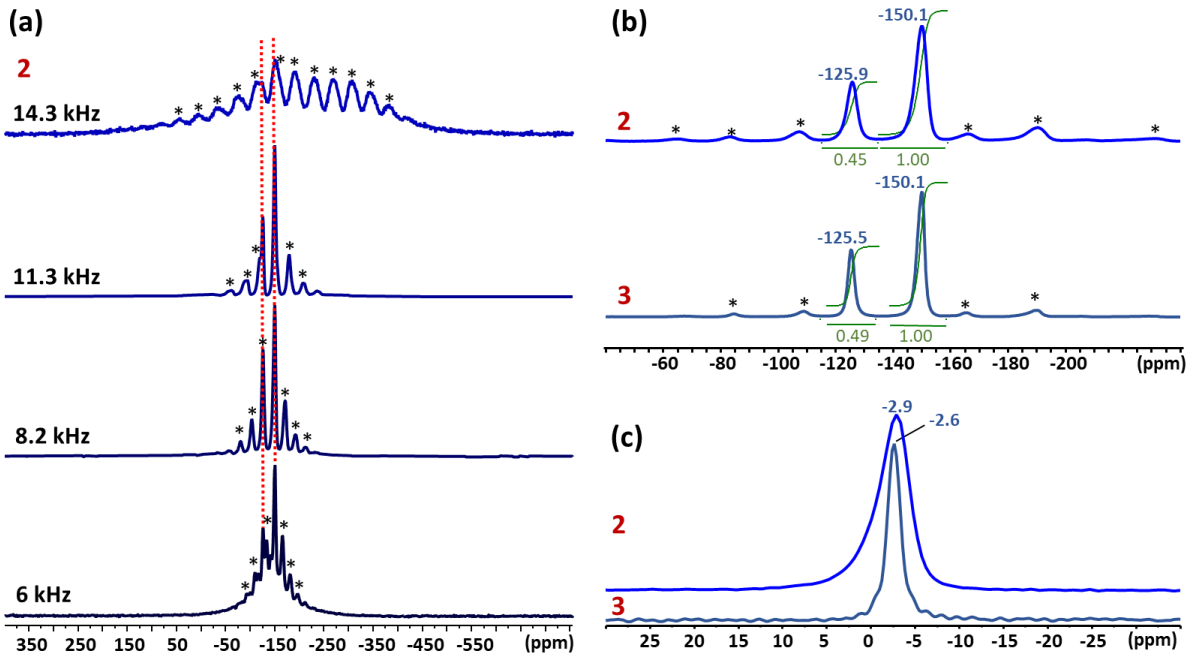

Figure 1: Selected MAS NMR spectra for sample **2** and **3**: (a) ^{19}F Hahn-echo of **2** at 295 K and different ν_r, (b) ^{19}F Hahn-echo and (c) ^{11}B of **2** and **3** at 253 K and ν_r =15.6 and 15.4 kHz.

* = spinning sidebands.

Clear separation of the isotropic signals can be obtained with a spinning rate of 15.6 kHz while using a cold flux of air to reduce the temperature inside the sample. The ^{19}F MAS Hahn-echo spectra acquired with an external temperature of 253 K exhibit clear isotropic resonance corresponding to the BF_4^- and SiF_6^{2-} anion located at -150.1 ppm and -125.9 ppm, respectively, in agreement with earlier studies [43,44]. Separation of resonance allowed us to obtain good integrations and the corresponding SiF_6^{2-}/BF_4^- intensity ratio of 0.45±0.02 and 0.49±0.02 for sample **2** and **3**, respectively, which agrees with the composition issued from elemental analyses. The ^{11}B MAS NMR spectrum obtained at low temperature shows isotropic resonances at -2.9 and -2.6 ppm for the BF_4^- anion in **2** and **3**, respectively, consistent with the literature [43]. It can also be noted that the ^{19}F and ^{11}B signals of **2** are broader than those of **3** and that the ^{19}F spinning sidebands, due mostly to chemical shift anisotropy, of **2** are stronger than for **3**. These can be related to a less homogeneous composition and morphology of the latter and possibly the presence of a small amorphous phase explaining the disordered spin crossover behaviour (*vide infra*).

The homogeneity and the spin crossover properties of the samples were probed by optical reflectivity and magnetic measurement (see **Figure 2** and SI). As already reported, **1** exhibits a multistep transition centered at 250 K with a 20 K hysteresis loop [26]. This behavior is associated with the presence of distinct crystalline phases. It is interesting to notice that in agreement with the ^{19}F MAS NMR study (see **Fig. S3** in ESI) and the experimental conditions (no glass), sample **1** does not contain traces of SiF_6^{2-} which could explain the independent crystalline domains and the multistep spin transition. In agreement with their close chemical composition, samples **2** and **3** present slightly different spin transition temperatures, but the behavior is drastically diverse (**Figure 2**). Indeed, the profile of the thermal variation of the magnetic measurement for **2** is more gradual, asymmetric and stepped compare to sample **3** which shows, for the desolvated form, a first order abrupt transition with a hysteresis loop of

10 K with $T_{1/2}^{\uparrow}$ of 316 K and $T_{1/2}^{\downarrow}$ of 326 K. For both samples, completeness of the spin transition is suggested by the χT values at low and high temperatures, which are close to the expected ones for an iron(II) species.

It appears interesting to compare the transition temperature of such mixed-cation complex with the corresponding non-mixed parent ones. Surprisingly, the reported SCO behavior of the $Fe(NH_2Trz)_3(SiF_6)$ complex with a transition temperature around 250 K [45] is not in line with the general tendency observed for the mixed-ligand and mixed-metal counterparts for which the progressive dilution led to a concomitant shift of the transition temperatures in between those of the parent complexes [18-21].

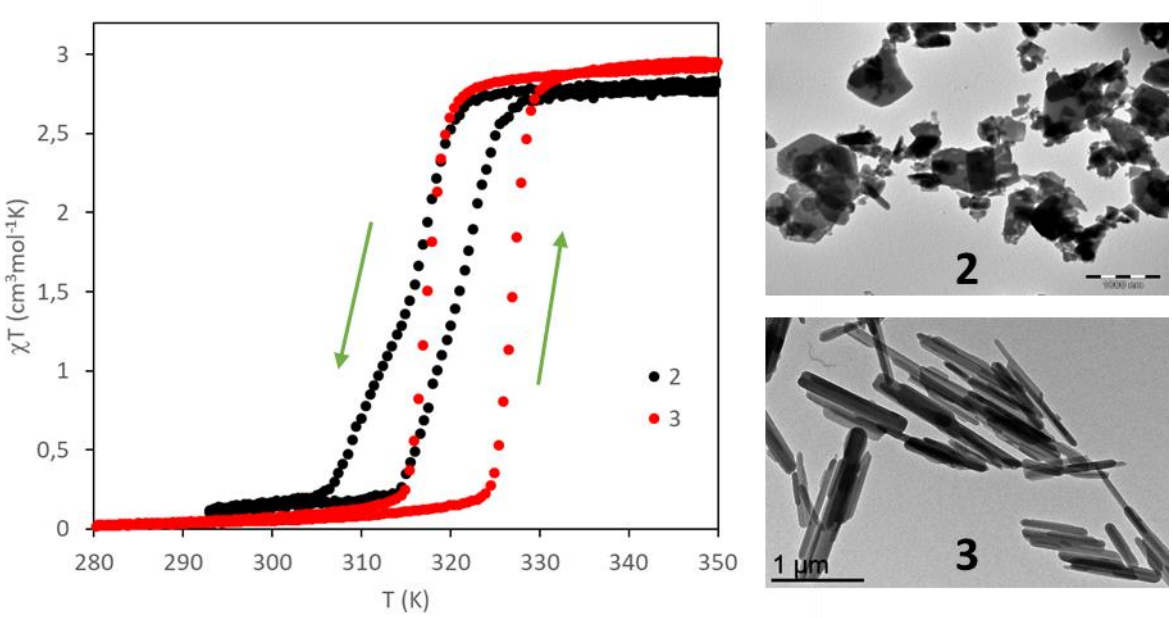

Figure 2: Thermal variation of the magnetic measurement (desolvated sample); arrows indicate the heating and cooling branches and selected TEM image for sample **2** and **3**

Powder X-ray diffraction measurements were performed on the different samples to compare notably their crystallinity and homogeneity. The precursor powder sample **1** shows a poor crystallinity with peak duplication, which is relevant for the multistep transition observed. In contrast, both sample **2** and **3** appear crystalline, although an amorphous fraction is suggested

for **2** by the ^{11}B NMR analysis. For both samples, the refinement of the unit cell from the diffractogramm is in agreement with the reported one for the corresponding crystal (space group: hexagonal P63/m) [26].

It seems that all samples are isostructural although the broadening of the peaks and the presence of additional peaks leave the doubt for sample **1**. Moreover, in agreement with the more chaotic spin crossover behavior for **2**, some splitting of peaks can be seen (see peak at $2\theta = 16°$). Such difference can be understood by the comparison of the composition of the samples and taking into account the crystal packing of the complex [26]. Indeed, the crystal arrangement of the 1D chains is complemented by two crystallographically independent anionic BF_4^- sites for **1** which balance the positive charges of the iron centers. Thus, like the crystal structure of **2** and **3** appears very close to that of **1**, the greatest difference between these compounds concerns the two anionic sites with two BF_4^- for $[Fe(NH_2trz)_3](BF_4)_2$ that are replaced by one BF_4^-/SiF_6^{2-} and one BF_4^-/--- for $[Fe(NH_2trz)_3](BF_4)_{2-x}(SiF_6)_{x/2}$. It comes out that the reduced cation exchange in sample **2,** with only 0.4 SiF_6^{2-} instead of 0.5 for **3**, generates "defects" in the crystal structure, which could explain the non-monotonous character of the spin transition for **2** although a mixture of composition is not exclude. Thus, the PSM approach lead to a more crystalline and more homogeneous $[Fe(NH_2trz)_3](BF_4)_1(SiF_6)_{0.5}$ sample.

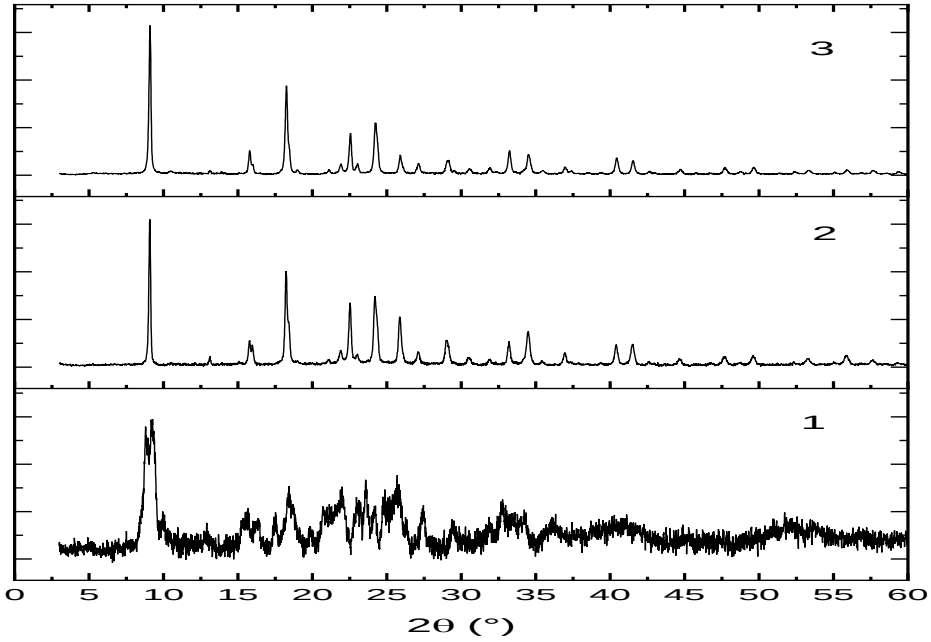

Figure 3: Powder X-ray diffractogram of samples **1-3** recorded at room temperature.

To complete the study, the size and morphology of the grains forming the powder were probed for all samples by transmission electronic microscopy (TEM). As expected for the synthesis of bulk samples, rather inhomogeneous particles in size and morphology are obtained for **1** and **2** (see **Fig. 2** and ESI). On the other hand, starting from the micrometric platelet objects in **1**, the cation exchange PSM reaction affords homogeneous rod like microparticles (1 µm long) visualized for sample **3.** Such surprising morphological reorganization was already observed for similar solid-liquide PSM reaction in this family of compounds [38]. These results agree with the proposed mechanism which implies that polar solvent (like water used in our experiments), thanks to stronger interactions with the Fe-triazole polymeric chains that constitute crystallites, can favour their separation promoting the cation exchange and the observed solid-solid restructuration. This hypothesis is also supported by the quite important distance between neighboring chains of 11.34 Å reported for the parent complex **1** [26].

4. Conclusions

PSM method appears to be a powerful approach to obtain crystalline and homogeneous coordination chemistry samples. Indeed, in doing so, for the first time we report the synthesis and the spin crossover properties of a pure mixed-anion complex belonging to the archetypal 1D chains "Fe-triazole" family of compounds. Moreover, this solid-liquid post synthetic modification reaction led to the stabilization of homogeneous rod like particles which stems from the ability of the 1D iron chains to be separated in polar solvent. The resulting $Fe(NH_2trz)_3(BF_4)(SiF_6)_{0.5}$ complex presents an abrupt spin crossover with a 10 K hysteresis loop centred just above room temperature (320 K) which makes this compound rather unusual and adequate for its integration into devices for future various applications. In particular, the fact that this compound presents a significant and anisotropic character of the unit cell parameters change as well as an anisometric morphology of the microparticles, makes it a good candidate for mechanical actuation purpose and the development of artificial muscles. [46]

Supporting Information

Supporting Information (thermogravimetric analysis, IR spectra, additional NMR spectra and optical reflectivity measurements) is available from the journal library or from the author.

Acknowledgments

This project has received funding from the European Research Council (ERC) under the European Union's Horizon 2020 research and innovation program (grant agreement No. 101019522). XY thanks the China Scholarship Council for a PhD grant.

References

1 O. Kahn and C. J. Martinez, Science, 1998, 279, 44–48.

2 A. Bousseksou, G. Molnar, L. Salmon and W. Nicolazzi, Chem. Soc. Rev., 2011, 40, 3313–3335.

3 M. A. Halcrow, ed., Spin-crossover materials: properties and applications, John Wiley & Sons, 2013.

4 K. S. Kumar, M. Ruben, Coord. Chem. Rev., 2017, 346, 176–205.

5 G.Molnar, S. Rat, L. Salmon, W. Nicolazzi and A. Bousseksou, Adv. Mater., 2018, 30, 1703862.

6 L. Cambi, A. Cagnasso, Atti. Accad. Naz Lincei, 1931, 13, 809.

7 M. A. Halcrow, I. Capel Berdiell, C. M. Pask, R. Kulmaczewski, Inorg. Chem. 2019, 58, 9811−9821

8 Olga Drath, Colette Boskovic, Coord. Chem. Rev., 2018, 375, 256.

9 K. Senthil Kumar, Y. Bayeh, T. Gebretsadik, F. Elemo, M. Gebrezgiabher, M. Thomas, M. Ruben, Dalton Trans., 2019, 48, 15321.

10 M.-L. Boillot, B. Weber, C. R. Chimie, 2018, 21, 1196.

11 D. J. Harding, P. Harding, W. Phonsri, Coord. Chem. Rev., 2016, 313, 38.

12 M. Carmen Munoz, J. A. Real, Coord. Chem. Rev., 2011, 255, 2068.

13 M. A. Halcrow, Chem. Soc. Rev., 2011, 40, 4119–4142.

14 P. Guionneau, Dalton Trans., 2014, 43, 382–393.

15 M. Attwood, H. Akutsu, L. Martin, T. J. Blundell, P. Le Maguere, S. S. Turner, Dalton Trans., 2021, 50,11843

16 O. Roubeau, Chem. Eur. J., 2012, 18, 15230 – 15244.

17 A. Sugahara, H. Kamebuchi, A. Okazawa, M. Enomoto, N. Kojima, Inorganics 2017, 5, 50.

18 L. G. Lavrenova, V. N. Ikorskii, V. A. Varnek, I. M. Oglezneva, S. V. Larionov, Zh. Strukt. Khim., 1993, 34(6), 145.

19 J. Krober, E. Codjovi, O. Kahn, F. Groliere and C. Jay, J. Am. Chem. Soc., 1993, 115, 9810–9811.

20 O. G. Shakirova, L. G. Lavrenova, Yu. G. Shvedenkov, V. N. Ikorskii, V. A. Varnek, L. A. Sheludyakova, V. L. Varand, T. A. Krieger, S. V. Larionov, J. Struct. Chem., 2000, 41(5), 790–797.

21 V. A. Varnek and L. G. Lavrenova, J. Struct. Chem., 1997, 38, 850–852.

22 E. Coronado, J. R. Galan-Mascaros, M. Monrabal-Capilla, J. Garciıa- Martınez and P. Pardo-Ibanez, Adv. Mater., 2007, 19, 1359–1361.

23 S. Titos-Padilla, J. M. Herrera, X.-W. Chen, J. J. Delgado, E. Colacio, Angew. Chem., Int. Ed., 2011, 50, 3290–3293.

24 I. Suleimanov, J. Sanchez Costa, G. Molna´r, L. Salmon, I. O. Fritsky, A. Bousseksou, Fr.-Ukr. J. Chem., 2015, 3(1), 66.

25 L. Salmon, L. Catala, Comptes Rendus Chim., 2018, 21, 1230–1269.

26 A. Grosjean, Matériaux polymèriques 1D à transition de spin : investigations structurales multi-échelles, HAL thesis, Université de Bordeaux, version 1, 2013.

27 I. Suleimanov, O. Kraieva, G. Molnar, L. Salmon, A. Bousseksou, Chem. Commun. 2015, 51, 15098.

28 I. Suleimanov, J. Sanchez Costa, G. Molnar, L. Salmon, A. Bousseksou, Chem. Commun. 2014, 50, 13015.

29 I. Suleimanov, O. Kraieva, J. Sanchez Costa, I. O. Fritsky, G. Molnar, L. Salmon, A. Bousseksou, J. Mater. Chem. C 2015, 3, 5026–5032.

30 R. Torres-Cavanillas, L. Lima-Moya, F. D. Tichelaar, H. W. Zandbergen, M. Giménez-Marqués, E. Coronado, Dalton Trans., 2019, 48, 15465.

31 Y. Zan, L. Salmon, A. Bousseksou, Nanomaterials, 2021, 11, 3169.

32 J. H. Askew and H. J. Shepherd, Dalton Trans., 2020, 49, 2966.

33 E. Resines-Urien, L. Piñeiro-López, E. Fernandez-Bartolome, A. Gamonal, M. Garcia-Hernandez, J. Sánchez Costa, Dalton Trans., 2020, 49, 7315

34 C.-F. Wang, R.-F. Li, X.-Y. Chen, R.-J. Wei, L.-S. Zheng, J. Tao, Angew. Chem., Int. Ed., 2015, 54, 1574–1577.

35 C. F. Wang, G. Y. Yang, Z. S. Yao and J. Tao, Chem. – Eur. J., 2018, 24, 3218–3224.

36 A. Enríquez-Cabrera, L. Routaboul, L. Salmon, A. Bousseksou, Dalton Trans., 2019, 48, 16853–16856.

37 A. Enriquez-Cabrera, K. Ridier, L. Salmon, L. Routaboul, A. Bousseksou, Eur. J. Inorg. Chem., 2021, 2000–2016.

38 A. Enrıquez-Cabrera, L. Getzner, L. Salmon, L. Routaboul, A. Bousseksou, New J. Chem., 2022, 46, 22004.

39 O. Kahn, J. Kröber, C. Jay, Advanced Materials, 1992, 4, 718.

40 Schmidt-Rohr, K.; Spiess, HW. Multidimensional solid-state NMR and polymers. Academic Press Inc.; San Diego: 1994.

41 Lowe, I. J. Physical Review Letters 1959, 2, 285.

42 Andrew, E. R.; Bradbury, A.; Eades, R. G. Nature 1959, 183, 1802.

43 J. W. Wiench, C. Michon, A. Ellern, P. Hazendonk, A. Iuga, R. J. Angelici, M. Pruski, J. Am. Chem. Soc., 2009, 131, 11801.

44 H.-M. Kao, Y.-C. Chen, J. Phys. Chem. B 2003, 107, 3367.

45 O. G. Shakirova, M. Grunert, D. Yu. Naumov, F. Gütlich, L. G. Lavrenova, J. Struct. Chem., 2010, 51, 1, 45-52.

46 Y. Zan, M. Piedrahita-Bello, S. E. Alavi, G. Molnár, B. Tondu, L. Salmon, A. Bousseksou, Adv. Intell. Syst. 2023, 2200432.